JOURNAL OF GEOPHYSICAL RESEARCH, VOL. 85, NO. B12, PAGES 7235–7241, DECEMBER 10, 1980

Geoid Height Versus Age for Symmetric Spreading Ridges

DAVID SANDWELL AND GERALD SCHUBERT

Department of Earth and Space Sciences, University of California at Los Angeles, Los Angeles, California 90024

Geoid height–age relations have been extracted from Geos 3 altimeter data for large areas in the North Atlantic, South Atlantic, southeast Indian, and southeast Pacific oceans. Except for the southeast Pacific area, geoid height decreases approximately linearly with the age of the ocean floor for ages less than about 80 m.y. in agreement with the prediction of an isostatically compensated thermal boundary layer model (Haxby and Turcotte, 1978). The geoid-age data for 0 to 80 m.y. are consistent with constant slopes of -0.094 ± 0.025, -0.131 ± 0.041, and -0.149 ± 0.028 m/m.y. for the South Atlantic, southeast Indian, and North Atlantic regions, respectively. For ages greater than 80 m.y. the geoid-age relation for the North Atlantic is nearly flat, indicating a reduction in the rate of boundary layer thickening with age. The uncertainties in the geoid slope–age estimates are positively correlated with spreading velocity.

INTRODUCTION

It has long been recognized that the horizontally rigid plates sliding across the earth are the surface expressions of large-scale mantle convection. The plates themselves are thermomechanical boundary layers associated with convection at highly supercritical Rayleigh number [*Turcotte and Oxburgh,* 1967; *Schubert,* 1979]. The density variations associated with the lithospheric boundary layer contribute significantly both to the forces driving the plates [*Hager,* 1978; *Schubert,* 1980] and to the departures in the shape of the earth (geoid) from hydrostatic equilibrium [*Kaula,* 1972]. Density anomalies not associated with the thermal structure of the lithosphere also contribute to the geoid and tend to mask the lithospheric signal.

A theoretical lithospheric geoid signal has been derived by *Haxby and Turcotte* [1978] by using a long-wavelength, flat earth approximation to the geoid height N of an isostatically compensated thermal boundary layer:

$$N = \frac{-2\pi G \rho_m{}^{\alpha}(T_m - T_0)\kappa}{g}\left[1 + \frac{2\rho_m \alpha (T_m - T_0)}{(\rho_m - \rho_w)\pi}\right] t \quad (1)$$

where g is the acceleration of gravity, G is the gravitational constant, α is the thermal expansion coefficient, $(T_m - T_0)$ is the temperature difference across the surface thermal boundary layer, κ is the thermal diffusivity, ρ_m is mantle density, ρ_w is seawater density, and t is the age of the crust. Equation (1), which is based on the indefinite growth of a thermal boundary layer at the upper boundary of a cooling semi-infinite half space, predicts that geoid height should decrease linearly with increasing crustal age. *Chapman* [1977] has found that geoid height decreases with crustal age for individual tracks of Geos 3 data crossing the southwest Indian ridge. A similar decrease has also been observed [*Haxby and Turcotte,* 1978; *Haxby,* 1979] for tracks of Geos 3 data that cross a number of spreading ridges, including one that crosses the northern Mid-Atlantic Ridge. That particular track shows a decrease consistent with a linear geoid height–age relation of slope -0.16 m/m.y. for ages less than 50 m.y. For at least this one track it is apparent that the part of the geoid due to density anomalies associated with lithospheric cooling and subsidence is dominating the overall convective signal. However, as we will see in the following section, a geoid height–age dependence is not usually apparent when observed geoid height contours are superimposed on isochrons of the world's oceans. Thus the signal of the isostatically compensated oceanic lithosphere is hidden in the observed geoid. It is not even clear that this signal can be extracted from the data, since its predicted magnitude is 10–15 m (see the model results of Figure 7) while typical geoid undulations are 33 m [*Kaula,* 1966]. We will show that the lithospheric contribution to the geoid can be obtained from observations. Moreover, we will demonstrate that the signal is consistent with the theoretical linear geoid height–age relation for young ages but deviates from it for ages greater than 80 m.y.

Our study is made possible by the extensive oceanic coverage of the Geos 3 altimeter. These sea surface measurements are ideally suited to the study of the variations of the gravitational potential over spreading ridges because the signal-to-noise ratio of these data is near its peak for wavelengths between 800 and 4000 km. In contrast, the signal-to-noise ratio for shipboard gravity measurements is low in this wavelength interval [*Chapman and Talwani,* 1979].

DATA ANALYSIS

Sea surface heights averaged over 1° by 1° areas were obtained from processed Geos 3 altimeter data [*Rapp,* 1979]. The relatively small deviations between the sea surface and the geoid caused by oceanic circulation were neglected in this analysis. Age data taken from *Pitman et al.* [1974] were averaged over 2° by 2° areas since there was insufficient resolution for reliable 1° by 1° averages. Crustal ages for 2° by 2° areas in the Cretaceous quiet zone (85–110 m.y.) were obtained by linearly interpolating between magnetic lineations. Four oceanic regions containing both geoid and age data were chosen for study. The boundaries of these regions were adjusted to insure that equal areas of seafloor were contained within each 5 to 10 m.y. time interval on either side of the ridge. Figure 1 shows the outline of each area. The velocity vectors indicate present-day plate motions [*Minster and Jordan,* 1978].

Figure 2 shows a contour map of the geoid (heavy lines) superimposed upon age contours (dashed lines) for the region in the South Atlantic. There is no geoid height–age relationship obvious on the basis of a visual inspection of these contours. If geoid height were strictly related to age, the contours would be parallel, and geoid heights would be symmetric about the ridge. However, a large-amplitude long-wavelength geoid undulation, trending roughly NW to SE, effectively masks the age-dependent signal. Geoid height and age contours in either

Paper number 80B0926.
0148-0227/80/080B-0926$01.00

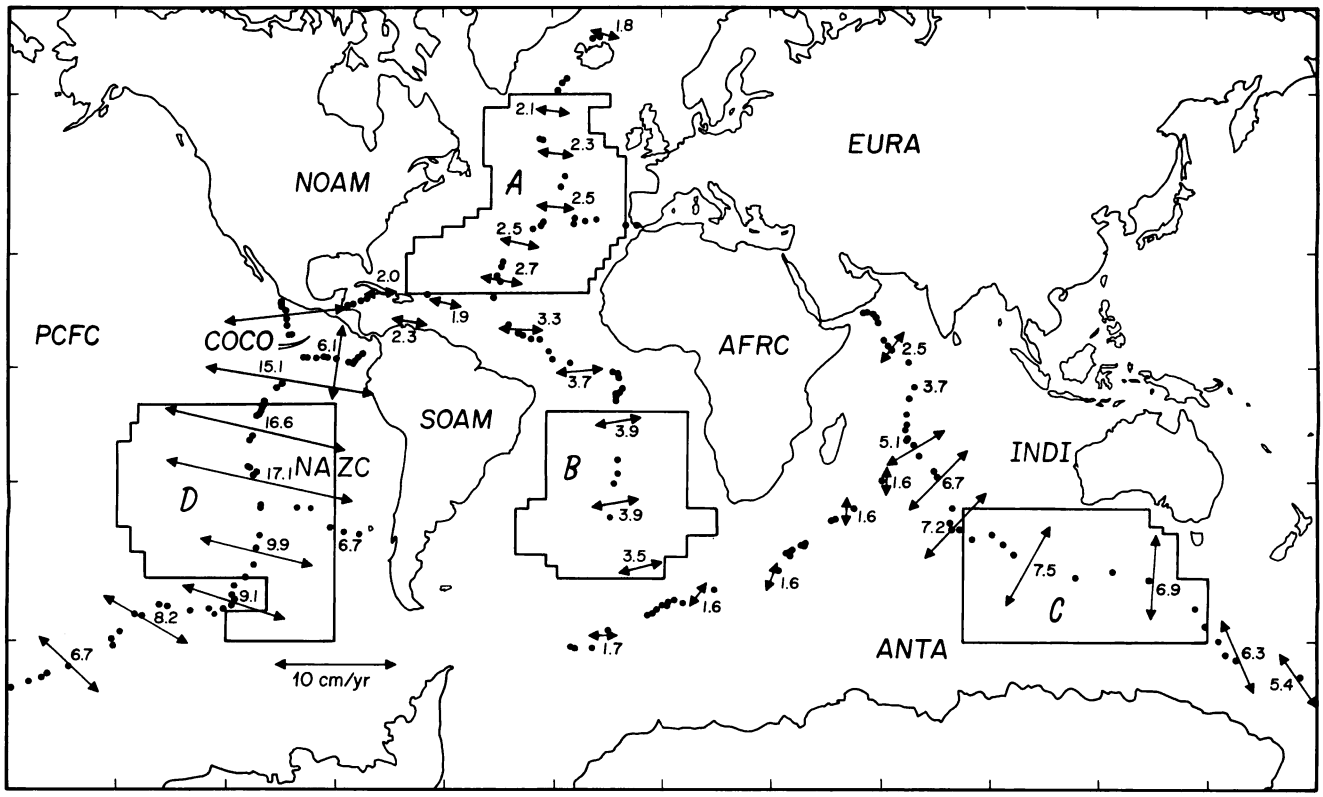

Fig. 1. World map outlining areas chosen for geoid height–age analysis. Dots represent earthquake epicenters. Arrows are present-day spreading velocities [*Minster and Jordan*, 1978].

the southeast Pacific or the southeast Indian Ocean areas outlined in Figure 1 also have no apparent visual correlation. In the area of the North Atlantic (Figure 1), though geoid height contours are symmetric about the ridge, they are not parallel to isochrons because of a long-wavelength trend in the geoid parallel to the ridge (Figure 3).

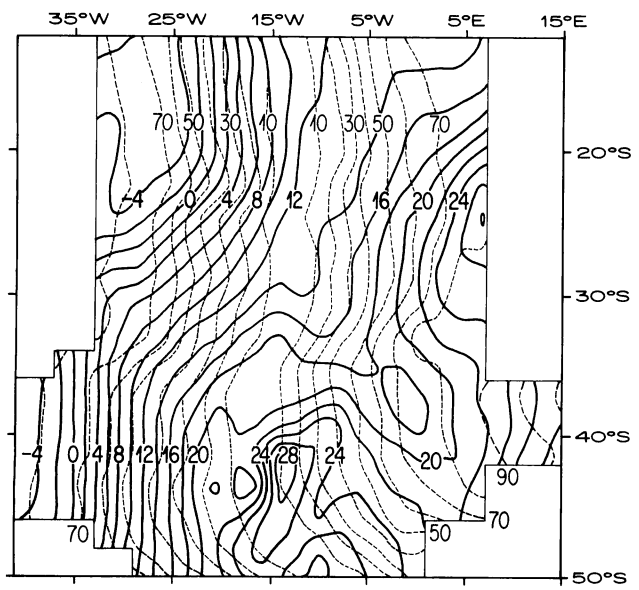

Fig. 2. Geoid height contours (solid curves) and isochrons (dashed curves) superimposed for a large portion of the South Atlantic. Geoid heights are contoured at 2 m intervals and ages are contoured at 10-m.y. intervals. Geoid height contours were made from digitized 2° × 2° averages.

In order to extract a geoid height–age relation from the data we have calculated the time rate of change of geoid height in the direction of increasing age. This procedure eliminates geoid height variations parallel to the isochrons. Long-wavelength antisymmetric trends across the ridge can be removed by averaging geoid slopes over equal areas within a given time interval on either side of the ridge [*Chapman*, 1977]. The slope of the geoid in the direction of increasing age $\partial N/\partial t$ is obtained by taking the scalar product of the horizontal gradient of geoid height $\nabla_h N$ with the horizontal gradient of crustal age $\nabla_h t$:

$$\frac{\partial N}{\partial t} = \frac{\nabla_h N \cdot \nabla_h t}{\nabla_h t \cdot \nabla_h t} \tag{2}$$

Age gradients were computed on a 2° by 2° grid using a first difference formula and the 2° by 2° average age data. A geoid height gradient was obtained at the same point as an age gradient by determining the slope of the plane which best fit the 16 nearest 1° by 1° geoid height determinations. Geoid slopes on the 2° by 2° grid were then calculated from (2). These individual slopes were weighted by the latitude-dependent area of each 2° by 2° square before averaging the slopes within a given time interval. The slope of any 2° by 2° area that straddled a ridge was not included. Most slope estimates were based on averages over 10 to 40 times the area in a 2° by 2° square at the equator. The standard deviations of the average slope estimates were also computed from the individual slopes within each time interval. The magnitudes of the standard deviations are measures of the contributions of density anomalies not directly related to age to the mean slope estimates.

The 2° grid spacing used above eliminates geoid undula-

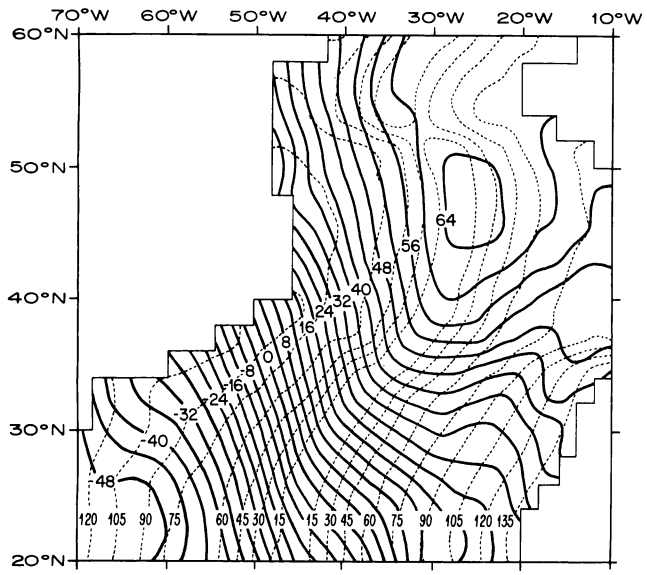

Fig. 3. Geoid heights (solid curves) superimposed on age contours (dashed lines) for a region of the North Atlantic. The geoid is contoured at 4-m intervals, and ages are contoured at 15-m.y. intervals.

tions and age variations with wavelengths shorter than several hundred kilometers. The gradient operation prewhitens the data by dividing their spectra by the wavelength. This suppresses the longest wavelengths and removes the mean.

RESULTS

Time rates of change of geoid height in the direction of increasing age for all four oceanic areas are shown in Figure 4. Each data point is the average geoid slope within either 5 m.y. time intervals for the southeast Pacific (Figure 4*d*) and southeast Indian (Figure 4*c*) Ocean areas or 10 m.y. time intervals for the North Atlantic (Figure 4*a*) Ocean and South Atlantic (Figure 4*b*) Ocean areas. The vertical bars represent 1 standard deviation of the mean. Each dashed horizontal line is the best fitting (in the least squares sense) constant slope approximation to the geoid-age relations for ages less than 80 m.y. The maximum ages range from 50 m.y. for the southeast Indian Ocean area to 130 m.y. for the North Atlantic Ocean area. The upper limits on ages within each area were set by the availability of symmetric age data. Figure 5 shows the geoid height versus age curves for the four oceanic areas obtained by integrating the mean values of the geoid slope versus age data of Figure 4. Table 1 is a compilation of all the data shown in Figures 4 and 6.

North Atlantic

The slope estimates for the North Atlantic are negative and statistically different from zero for ages less than 80 m.y. The estimates for greater ages are close to zero and have relatively small uncertainties. A best fitting constant slope was determined to test the prediction of (1). For the 0 to 80 m.y. age interval the mean of the slope estimates weighted by the inverse of their variances is -0.149 ± 0.028 m/m.y. The constant slope approximation lies within 1 standard deviation of all the slope-age estimates between 0 and 50 m.y. (Figure 4*a*). The data in the interval 50 to 80 m.y. are not closely approximated by the best fitting constant slope. However, these data have relatively large uncertainties, and therefore they have relatively little influence on the value of the best fitting constant slope.

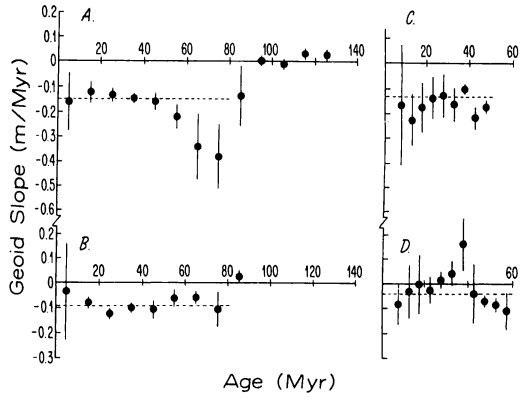

Fig. 4. Estimates of the slope of the geoid in the direction of increasing age, as a function of age, for each of the four oceanic regions outlined in Figure 1. Error bars represent 1 standard deviation. Dashed line is the best fitting constant slope between 0 and 80 m.y. (*a*) North Atlantic, (*b*) South Atlantic, (*c*) SE Indian, (*d*) SE Pacific.

The individual slopes contributing to the mean slope estimates between 50 and 80 m.y. have a nearly bimodal distribution; i.e., they cluster into two groups on either side of the mean. The group with the more negative slopes derives from the region north of 30°N. The portion of this region between the 70-m.y. isochrons (Figure 3) contains both broad residual depth and gravity anomalies [*Sclater et al.*, 1975; *Cochran and Talwani*, 1977, 1978]. We believe that the anomalous slope in the topography along the perimeter of the residual depth anomaly causes the anomalous geoid slopes in the 50 to 80 m.y. age interval. To substantiate this hypothesis, we computed separate slope estimates for the region lying north of 30°N (Figure 6, solid circles) and for the region lying south of 32°N (Figure 6, open circles). Within the 50 to 80 m.y. age interval the slope estimates for the two regions are quite different.

The integral of the slope-age data for the entire North Atlantic (solid line, Figure 5) yields a drop of 18 m in 90 m.y. If the data north of 32°N are excluded, the drop in the geoid height is only 12.5 m in 90 m.y.

South Atlantic

The estimates of geoid slope are nearly constant in the 0 to 80 m.y. age interval. The best fitting linear geoid slope–age re-

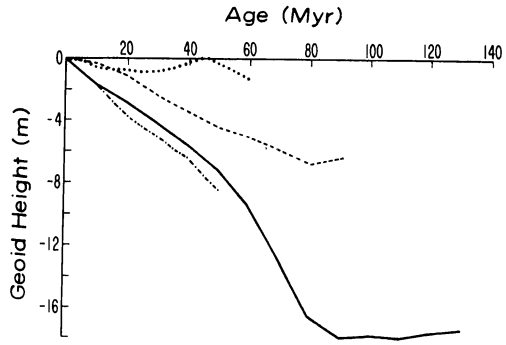

Fig. 5. Geoid height–age relations obtained by integrating the slope estimates of Figure 4. North Atlantic (solid line), South Atlantic (dashed line), SE Indian (dash-dot line), SE Pacific (dotted line).

TABLE 1. Average Geoid Slopes

	t, m.y.												
	5	15	25	35	45	55	65	75	85	95	105	115	125
						North Atlantic							
A	8.3	28.5	21.2	17.8	24.2	30.3	37.2	38.6	26.6	18.0	19.0	13.0	10.5
$\langle \partial N/\partial t \rangle$	−0.161	−0.121	−0.133	−0.146	−0.160	−0.220	−0.341	−0.380	−0.138	0.012	−0.008	0.031	0.028
σ	0.115	0.040	0.025	0.010	0.029	0.047	0.113	0.131	0.119	0.018	0.017	0.013	0.018
						North Atlantic (North of 30°N)							
A	4.8	18.8	15.0	11.7	18.0	23.2	26.5	27.0	16.8	7.3	6.6		
$\langle \partial N/\partial t \rangle$	−0.192	−0.129	−0.142	−0.133	−0.173	−0.264	−0.358	−0.484	−0.206	0.007	−0.048		
σ	0.062	0.030	0.016	0.008	0.021	0.041	0.071	0.100	0.146	0.016	0.023		
						North Atlantic (South of 32°N)							
A	4.4	12.3	7.1	7.0	7.9	8.7	12.4	13.3	12.3	13.1	15.0	11.4	9.7
$\langle \partial N/\partial t \rangle$	−0.190	−0.133	−0.111	−0.159	−0.113	−0.096	−0.274	−0.148	−0.020	0.009	−0.022	0.033	0.040
σ	0.168	0.056	0.041	0.012	0.039	0.037	0.191	0.107	0.048	0.020	0.017	0.014	0.018
						South Atlantic							
A	35.6	36.0	24.9	29.6	32.6	29.0	35.4	58.0	27.7				
$\langle \partial N/\partial t \rangle$	−0.033	−0.079	−0.123	−0.102	−0.106	−0.062	−0.060	−0.106	0.025				
σ	0.194	0.022	0.019	0.018	0.034	0.035	0.024	0.070	0.022				
	t, m.y.												
	2.5	7.5	12.5	17.5	22.5	27.5	32.5	37.5	42.5	47.5	52.5	57.5	62.5
						Southeast Indian Ocean							
A	27.0	38.2	25.0	25.9	21.0	24.4	19.7	15.2	9.0	8.8			
$\langle \partial N/\partial t \rangle$	0.196	−0.168	−0.227	−0.176	−0.138	−0.129	−0.165	−0.104	−0.219	−0.174			
σ	0.610	0.241	0.102	0.098	0.084	0.086	0.065	0.013	0.043	0.022			
						Southeast Pacific							
A	62.5	70.2	77.7	60.7	44.0	37.7	39.8	31.4	17.4	12.9	5.5	2.3	
$\langle \partial N/\partial t \rangle$	−0.031	−0.084	−0.031	−0.002	−0.026	0.014	0.042	0.162	−0.038	−0.071	−0.084	−0.109	
σ	0.225	0.081	0.106	0.118	0.052	0.029	0.049	0.107	0.118	0.023	0.029	0.074	

A is the area normalized by a 2° by 2° square at the equator; $\langle \partial N/\partial t \rangle$ is the mean geoid slope in m/m.y.; σ is the standard deviation in m/m.y.

lation for the South Atlantic, −0.094 ± 0.025 m/m.y., lies within 1.25 standard deviations of all of the slope estimates in the age range 0 to 80 m.y. (Figure 4*b*). The one slope estimate for ages greater than 80 m.y. is nearly zero. The relatively small uncertainties in the data and the good overall fit of the constant slope approximation to the geoid height–age relation between 0 and 80 m.y. indicate that a linear geoid height–age relation is consistent with the data from the entire South Atlantic. The integral of the slope–age estimates (dashed line in Figure 5) has a 6 m decrease in the 0 to 80 m.y. time span.

Southeast Indian Ocean

The available data for this area extend only to 50 m.y., and the uncertainties in most of the slope estimates are larger than in the Atlantic regions (Figure 4*c*). The best fitting constant slope of −0.131 ± 0.041 m/m.y. lies an average of 1.3 standard deviations away from the data. Integration of the slope estimates yields a geoid height–age relation (dash-dot line in Figure 5) with an 8.5 m decrease in 50 m.y.

Southeast Pacific

In contrast to the other oceanic areas, geoid height in the southeast Pacific region does not appear to decrease with age (Figure 4*d*). The overall drop in geoid height (dotted line in Figure 5) between the ages of 0 and 60 m.y. is only 1.5 m. The best fitting constant slope of −0.041 ± 0.054 m/m.y. lies more than 1 standard deviation away from 5 of the 11 slope estimates. The data within the 20 to 45 m.y. interval are incompatible with a geoid height–age relation of constant negative slope. The slope–age data in this age band reflect the geoid high centered over the Peru-Chile trench. In general, the free air gravity high associated with a subduction zone and its outer rise extends no more than a few hundred kilometers seaward of the trench axis [*Watts and Talwani*, 1974]. However, all major subduction zones have a geoid high extending roughly 2000 km [*McAdoo*, 1980] from the trench with an amplitude of more than 20 m [*Rapp*, 1979]. The geoid anomaly associated with the Peru-Chile trench contributes positive values to slope estimates for seafloor with ages between 10 and 45 m.y. on the east side of the east Pacific rise. As a result, the decrease in geoid height associated with lithospheric cooling is effectively offset in this age interval by the increase in geoid height with proximity to the trench. The failure to extract a meaningful geoid height–age relation in the southeast Pacific could also be due to the complicated ridge geometry, i.e., the presence of a triple junction, and to the presence of fossil spreading ridges.

Discussion and Summary

The general results of the geoid slope–age analysis are the following:

1. Geoid height–age relations associated with lithospheric cooling can be extracted from the observed geoid over oceanic areas.

2. The North Atlantic, South Atlantic, and southeast Indian Ocean regions all have geoid heights which decrease nearly linearly with age for ages less than about 80 m.y., consistent with the signature of an isostatically compensated cooling lithospheric plate.

3. The slope of the geoid in the direction of increasing age is close to zero in the North Atlantic for ages greater than 80 m.y. Only one data point is available for the South Atlantic for ages exceeding 80 m.y. At 85 m.y. the geoid slope in the South Atlantic is also close to zero.

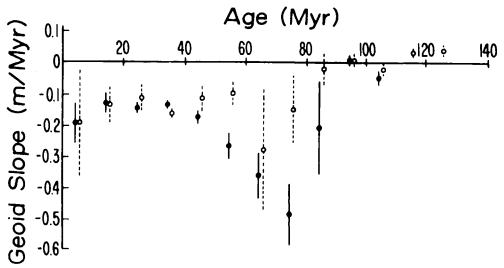

Fig. 6. Estimates of the slope of the geoid in the direction of increasing age, as a function of age, for the North Atlantic north of 30°N (solid circles) and south of 32°N (open circles). The error bars represent 1 standard deviation. The region north of 30°N contains a broad residual depth anomaly.

4. Geoid undulations that are unrelated to crustal age cannot be completely removed by the above data analysis technique.

One other conclusion that can be drawn from Figures 1 and 4 is that the uncertainties in the geoid slope estimates have a positive correlation with spreading velocity. This correlation was unexpected, but in retrospect it is easy to explain. Uncertainties in the slope estimates arise from geoid anomalies that are unrelated to age. Since fast spreading ridges (half-rate 3–10 cm/yr) have more seafloor area per time interval than slow spreading ridges (half-rate 0–3 cm/yr), there are more age-independent geoid anomalies per time interval in the faster spreading oceans. When this is combined with the fact that the change in geoid height per time interval is nearly independent of spreading velocity, it is not surprising that this uncertainty-velocity correlation exists. This observation suggests that the best geoid height–age results will come from a reanalysis of the southwest Indian ridge by using more data than were available to *Chapman* [1977].

Through (1), the slopes of the observed geoid height–age relations (Figure 4) can be used to constrain the value of the product $\alpha\kappa(T_m - T_0)$ appropriate to the oceanic upper mantle. The values of α, κ, and $T_m - T_0$, derived from the empirical depth-age and heat flow–age relations for the North Atlantic [*Parsons and Sclater*, 1977], yield a slope of −0.16 m/m.y. This lies within the error bounds of the best fitting constant geoid slope-age relations (ages < 80 m.y.) for both the North Atlantic and southeast Indian oceans. For the South Atlantic a slope of −0.16 m/m.y. falls below all of the uncertainties in the 0 to 80 m.y. slope estimates. More work needs to be done in this region to determine if the depth, heat flow, and geoid data are mutually consistent with the isostatically compensated thermal boundary layer cooling model. The lithospheric cooling model cannot explain the observed geoid slope–age relation for the southeast Pacific region. Since this relation (Figure 4*d*) is significantly different from the observed geoid slope–age relations of the other three regions, we believe that the lithospheric cooling signal was not successfully extracted from the geoid observations in the southeast Pacific. The geoid anomaly associated with the Peru-Chile trench and the complications associated with the presence of a triple junction and a fossil spreading center in the area of study contribute to the difficulty in deducing the lithospheric geoid signal in the southeast Pacific.

The observed flattening in the geoid height–age relation for

ages greater than 80 m.y. in the North Atlantic cannot be explained by the boundary layer cooling model. Accordingly, we have investigated the possibility that the flattening might be understood in terms of a plate cooling model. In this model [see, e.g., *Parsons and Sclater,* 1977] a plate of constant thickness l cools to the surface; both the surface temperature T_0 and the temperature at the base of the plate T_m are held constant. *Parsons and Sclater* [1977] have given analytic formulas for the depth of the ocean $D(t)$ and the thermally induced density anomaly in the plate. These formulas together with the *Ockendon and Turcotte* [1977] approximation for the geoid height N can be used to derive the geoid height–age relation for the cooling plate model. The result is

$$N(t) = \frac{-2\pi G l^2}{g}\left\{(\rho_m - \rho_w)\frac{D^2(t)}{2} + \alpha\rho_m(T_m - T_0)\cdot\left(\frac{1}{6} + \frac{2}{\pi^2}\sum_{n=1}^{\infty}\frac{(-1)^n}{n^2}\exp(-n^2 c t)\right)\right\} \quad (3)$$

where

$$c = \pi^2\kappa/l^2 \quad (4)$$

$$D(t) = \frac{\alpha\rho_m(T_m - T_0)}{2(\rho_m - \rho_w)}\left(1 - \frac{8}{\pi^2}\sum_{n=1}^{\infty}\frac{\exp[-(2n-1)^2 c t]}{(2n-1)^2}\right) \quad (5)$$

A flat earth approximation and the neglect of horizontal heat conduction have been assumed in deriving (3).

Figure 7 shows geoid height versus age for the cooling plate model with $\kappa = 8 \times 10^{-3}$ cm^2/s, $\alpha = 3.1 \times 10^{-5}$ K^{-1}, ρ_m, = 3.33 g/cm^3, $\rho_w = 1.025$ g/cm^3, $T_m = 1365°$C, $T_0 = 0°$C, $l = 128$ km, and $g = 982$ cm/s^2. These parameter values are the same as those used by *Parsons and Sclater* [1977] for the North Atlantic. Figure 8 shows the geoid slope of this model as a function of age together with the data for the North Atlantic from Figure 4. The model shows a flattening in the geoid height–age relation and a geoid height which approaches 15 m at old ages (Figure 7). *Parsons and Richter* [1980] have shown that the ridge driving force can be related to the lithospheric geoid anomaly. For a geoid anomaly of about 15 m they obtain a driving force of about 3.5×10^{15} dyne/cm. The geoid slope–age relation of this particular model does not compare especially well with the data (Figure 8), which appear to show a more abrupt change from a nearly constant nonzero value of slope to an approximately zero value near 80 m.y.

The observed flattenings of the depth-age and heat flow–age [*Parsons and Sclater,* 1977] and geoid-age relations indicate that heat is being introduced into the base of the old oceanic lithosphere. Possible heat sources include shear heating [*Schubert et al.,* 1976] and small-scale convection [*Richter and Parsons,* 1975; *Parsons and McKenzie,* 1978]. To discriminate between these various models, the thermal boundary layer signal must be removed from the depth, heat flow, and geoid observations. The results of this study provide an empirical geoid height–age relation that can be removed from the geoid over large oceanic areas, so that the smaller scale upper mantle heat transfer mechanisms can be further investigated.

Finally, we note that significant extensions of this study may be possible by using age data from magnetic lineations identified since the *Pitman et al.* [1974] compilation and from Deep-Sea Drilling Project drill sites and ages inferred from rigid plate rotations. This would facilitate both higher resolution in areas already studied and inclusion of additional areas into the data base.

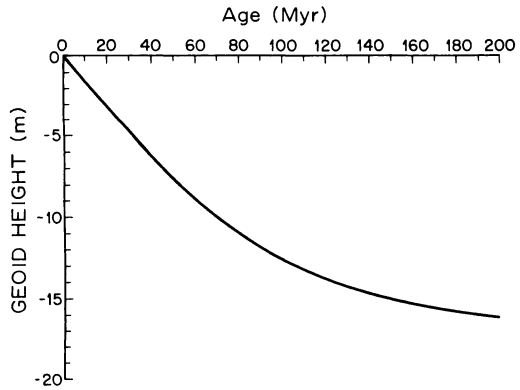

Fig. 7. Geoid height versus age for a cooling plate model of the oceanic lithosphere. The model and parameter values are described in the text.

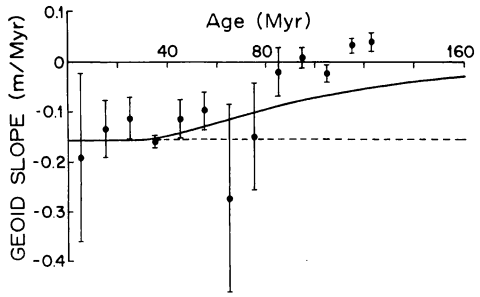

Fig. 8. Geoid slope versus age for the cooling plate model of Figure 7 together with the data for the North Atlantic from Figure 4.

Acknowledgments. We thank Richard Rapp for supplying 1° by 1° averages of the oceanic geoid and Brad Hager for helpful comments on an earlier version of this paper. This research was supported by the National Science Foundation under EAR 77-15198 and the National Aeronautics and Space Administration under NSG 5263.

REFERENCES

Chapman, M. E., Geoid anomaly over mid-ocean ridges (abstract), *Eos Trans. AGU, 58,* 368, 1977.

Chapman, M. E., and M. Talwani, Comparison of gravimetric geoids with Geos-3 altimetric geoid, *J. Geophys. Res., 84,* 3803–3816, 1979.

Cochran, J. R., and M. Talwani, Free-air gravity anomalies in the world's oceans and their relationship to residual elevation, *Geophys. J. R. Astron. Soc., 50,* 495–552, 1977.

Cochran, J. R., and M. Talwani, Gravity anomalies, regional elevation, and the deep structure of the North Atlantic, *J. Geophys. Res., 83,* 4907–4924, 1978.

Hager, B. H., Oceanic plate motions driven by lithospheric thickening and subducted slabs, *Nature, 276,* 156–159, 1978.

Haxby, W. F., The mid-ocean ridge geoid anomaly (abstract), *Eos Trans. AGU, 60,* 391, 1979.

Haxby, W. F., and D. L. Turcotte, On isostatic geoid anomalies, *J. Geophys. Res., 83,* 5473–5478, 1978.

Kaula, W. M., Tests and combination of satellite determinations of the gravity field with gravimetry, *J. Geophys. Res., 71,* 5303–5314, 1966.

Kaula, W. M., Global gravity and mantle convection, *Tectonophysics, 13,* 341–359, 1972.

McAdoo, D. C., Interpretation of geoid anomalies in the vicinity of subduction zones (abstract), *Eos Trans. AGU, 61,* 370, 1980.

Minster, J. B., and T. H. Jordan, Present-day plate motions, *J. Geophys. Res., 83,* 5331–5354, 1978.

Ockendon, J. R., and D. L. Turcotte, On the gravitational potential and field anomalies due to thin mass layers, *Geophys. J. R. Astron. Soc., 48,* 479–492, 1977.

Parsons, B., and D. McKenzie, Mantle convection and the thermal structure of the plates, *J. Geophys. Res., 83,* 4485–4496, 1978.

Parsons, B., and F. M. Richter, A relation between the driving force and geoid anomaly associated with mid-ocean ridges, *Earth Planet. Sci. Lett.*, in press, 1980.

Parsons, B., and J. G. Sclater, An analysis of the variation of ocean floor bathymetry and heat flow with age, *J. Geophys. Res., 82,* 803–827, 1977.

Pitman, W. C., R. L. Larson, and E. M. Herron, The age of the ocean basins, map, Geol. Soc. of Am., Inc., Boulder, Color., 1974.

Rapp, R. H., Global anomaly and undulation recovery using Geos-3 altimeter data, *Tech. Rep. 285,* Ohio State Dep. of Geod. Sci., Columbus, 1979.

Richter, F. M., and B. Parsons, On the interaction of two scales of convection in the mantle, *J. Geophys. Res., 80,* 2529–2541, 1975.

Schubert, G., Subsolidus convection in the mantles of terrestrial planets, *Ann. Rev. Earth Planet. Sci., 7,* 289–342, 1979.

Schubert, G., Self-driven motions of plates and descending slabs, in *Mechanisms of Plate Tectonics and Continental Drift*, edited by P. A. Davies and S. K. Runcorn, Academic, New York, 1980.

Schubert, G., C. Froidevaux, and D. A. Yuen, Oceanic lithosphere and asthenosphere: Thermal and mechanical structure, *J. Geophys. Res., 81,* 3525–3540, 1976.

Sclater, J. G., L. A. Lawver, and B. Parsons, Comparison of long-wavelength residual elevation and free air gravity anomalies in the North Atlantic and possible implications for the thickness of the lithospheric plate, *J. Geophys. Res., 80,* 1031–1052, 1975.

Turcotte, D. L., and E. R. Oxburgh, Finite amplitude convection cells and continental drift, *J. Fluid Mech., 28,* 29–42, 1967.

Watts, A. B., and M. Talwani, Gravity anomalies seaward of deep sea trenches and their tectonic implications, *Geophys. J. R. Astron. Soc., 36,* 57–90, 1974.

(Received March 3, 1980;
revised June 11, 1980;
accepted July 2, 1980.)